Band structure, quantum confinement, and exchange splitting in $Sc_{1-x}Er_xAs$ epitaxial layers buried in GaAs

S. J. Allen, Jr., F. DeRosa, C. J. Palmstrøm, and A. Zrenner*
Bellcore, Redbank, New Jersey 07701
(Received 17 October 1990)

Magnetotransport measurements have been used to explore the band structure of thin (20 nm) rare-earth monoarsenide ($Sc_{1-x}Er_xAs$, $x=0.57$ and 0.68) epitaxial films buried in GaAs. The Hall resistance and transverse magnetoresistance were measured in magnetic fields from 0 to 9 T and temperatures from 1.5 to 300 K. The results are successfully projected on a model of the band structure that predicts that the rare-earth monoarsenides are semimetals with holes at the zone center and pockets of electrons on the zone boundary at the X point. Below 20 K, Shubnikov–de Haas oscillations are assigned to the zone-boundary electrons. Remarkably, the angular dependence of the quantum oscillations is best understood by assuming that the electrons are quantum confined and experience only the normal component of the applied magnetic field. A large splitting of the zone-boundary electronic band structure is observed and attributed to the exchange interaction with the $4f$ moments localized on the Er ions.

I. INTRODUCTION

Recent experiments have shown that it is possible to grow heterostructures comprised of epitaxial metals or semimetals and III-V compound semiconductors such as GaAs.[1–15] It is expected that these systems will facilitate electronic and photonic technology as well as materials physics focused on electronics and photonics in low-dimensional metals and semimetals. In some instances these material systems are further embellished by being ferromagnetic or antiferromagnetic. To further our understanding of the electronic properties of these systems, we have used magnetotransport experiments to explore the band structure of thin epitaxial films of the rare-earth monoarsenides buried in GaAs.

The results that we describe here rely heavily on an existing band-structure calculation by Hasegawa and Yanase[16] for the Gd pnictides and this model calculation serves as an important guide to understanding the magnetotransport. Further, it was discovered that $Sc_{1-x}Er_xAs$ epitaxial layers that are closely lattice matched[17] to the GaAs substrate develop well-resolved Shubnikov–de Haas (SdH) oscillations at modest fields. These quantum oscillations taken with the temperature dependence of the Hall and transverse magnetoresistance provide a fairly stringent test of the aforementioned band structure and we conclude that the system is well described as a semimetal with electron and hole concentrations of $(3.1\pm0.1)\times10^{20}$ cm^{-3}. From the SdH oscillations we are able to deduce that the light electron effective mass is $m^*\approx0.17m_0$ and the exchange splitting of the conduction band caused by the interaction with the fully polarized localized $4f$ spin is 75 ± 5 meV. The angular dependence of the quantum oscillations is best understood in terms of quantum confinement despite the fact that the electron system has a relatively large electron or hole concentration and many electronic subbands in a 20-nm-thick film are occupied.

II. EXPERIMENT

The samples investigated here were grown by molecular-beam epitaxy (MBE).[17] They consisted of 500-nm undoped buffer of GaAs grown on a semi-insulating substrate followed by 20 nm of $Sc_{1-x}Er_xAs$. The rare-earth monoarsenide layer was capped by 50 nm of GaAs. The details of the growth conditions have been published elsewhere.[17]

Reflection high-energy electron-diffraction (RHEED) oscillations were used to calibrate the growth rate of ErAs and ScAs separately. The growth rate of the alloy, determined by RHEED oscillations, proved to be the sum of the individual growth rates of the pure layers. Table I shows the targeted composition and the one determined from RHEED oscillations, Auger-electron spectroscopy, and from Rutherford backscattering (RBS). The measured and targeted compositions agree within experimental error and throughout we will assume the targeted compositions.

The samples were patterned into Hall bars using conventional photolithographic techniques and wet chemical etching. The Hall resistance and transverse magnetoresistance was measured using both dc and ac techniques as a function of magnetic field from 0 to 9 teslas and temperature from 1.5 to 300 K. At low temperature the SdH oscillations were exposed by measuring the derivative of the transverse magnetoresistance as a function of magnetic field. Here the derivative was obtained by computing the derivative of the recorded data.

TABLE I. Targeted and measured composition of the $Sc_{1-x}Er_xAs$.

Sample	Targeted composition RHEED	Auger-electron spectroscopy	Rutherford backscattering
A	$Sc_{0.43}Er_{0.57}As$	$Sc_{0.47(5)}Er_{0.53(5)}As$	$Sc_{0.39(5)}Er_{0.61(5)}As$
B	$Sc_{0.32}Er_{0.68}As$	$Sc_{0.37(5)}Er_{0.63(5)}As$	$Sc_{0.32(5)}Er_{0.68(5)}As$

III. MAGNETOTRANSPORT

Figures 1 and 2 display the magnetoresistance for samples A and B as a function of magnetic field with temperature as a parameter. The most striking feature is the curvature and the change of the sign of the Hall resistance from "electron"-like to "hole"-like as the temperature is reduced from room temperature to liquid-helium temperatures. This is *prima facie* evidence that the transport is circumscribed by a compensated metal with nearly equal numbers of electrons and holes.

Shubnikov–de Haas oscillations appear in both samples discussed in this paper, but are not observed in pure ErAs films grown under similar conditions, despite the fact that the transport mobilities are not substantially higher in the $Sc_{1-x}Er_xAs$ alloys than the pure ErAs layers. It is possible, however, that by achieving a measure of lattice match between the $Sc_{1-x}Er_xAs$ and underlying GaAs substrate, the "grain" size of the epitaxial material is substantially larger and small-angle scattering from the boundaries is substantially reduced. Boundary scattering

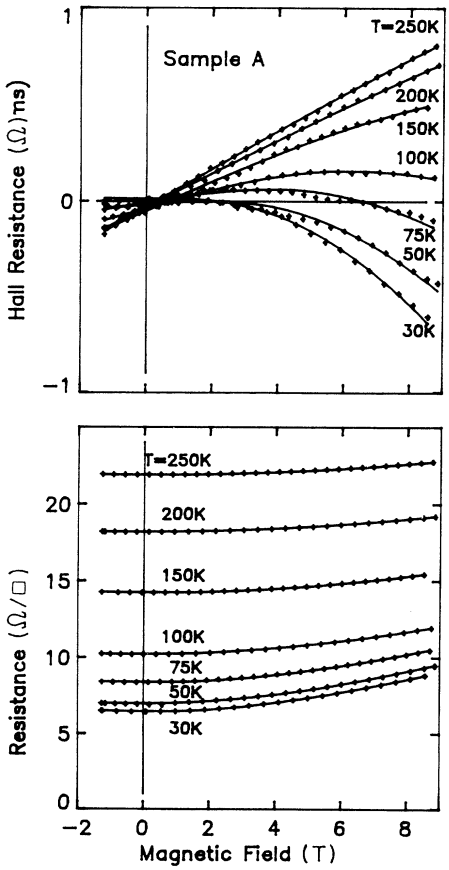

FIG. 1. Hall resistance and longitudinal magnetoresistance for sample A with temperature as a parameter. The solid lines are the result of a least-squares fit to the parameters shown in Fig. 8.

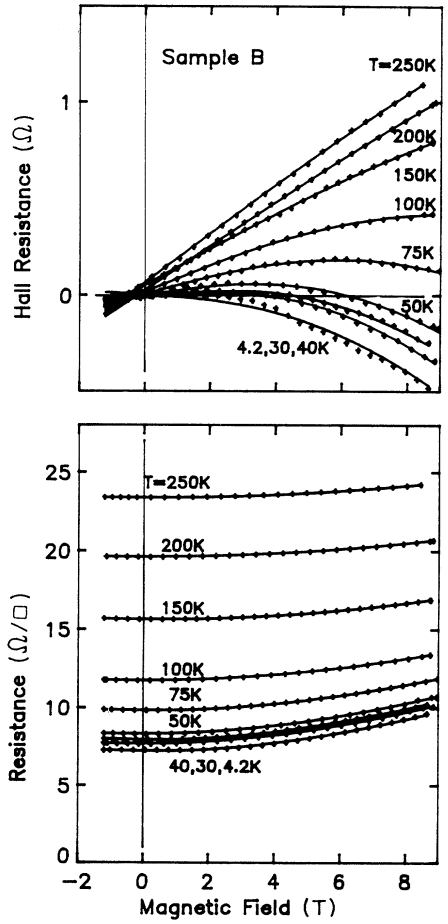

FIG. 2. Hall resistance and longitudinal magnetoresistance for sample B with temperature as a parameter. The solid lines are the result of a least-squares fit to the parameters shown in Fig. 9.

will have little effect on the transport mobilities but any scattering event effects the coherent cyclotron motion and suppresses quantum oscillations like the SdH oscillations described here. As a result we speculate that the lattice-matched layers have larger grains and more pronounced SdH oscillations despite showing no improvement in the transport mobility.

The SdH oscillations shown in Fig. 3 were recorded by differentiating $\rho_{xx}(B)$ numerically. To appreciate the scale of the quantum oscillations we display in Fig. 3 both $\partial\rho_{xx}/\partial B$ and $\rho_{xx}(B)$. The fractional changes in resistance produced by the oscillations are quite small when compared with those seen in the two-dimensional electron gas in semiconductors. Figure 3 also displays the SdH oscillations for sample B and we note that, despite the fact that the mobility of sample B is comparable to that of sample A, the amplitude of the oscillations in sample B is substantially diminished. The same comments can be made here with regard to the importance of grain-boundary scattering in limiting the amplitude of the quantum oscillations without having a dramatic effect on the apparent mobility.

The oscillations displayed in Fig. 3 can be Fourier analyzed and the results are shown in Fig. 4 for both samples A and B. The obvious beating that appears in the data is reflected in the appearance of two peaks in the Fourier transform. The frequencies that emerge for the two samples are the following.

Sample A: 330±5 and 385±5 T .

Sample B: 320±5 and 400±5 T .

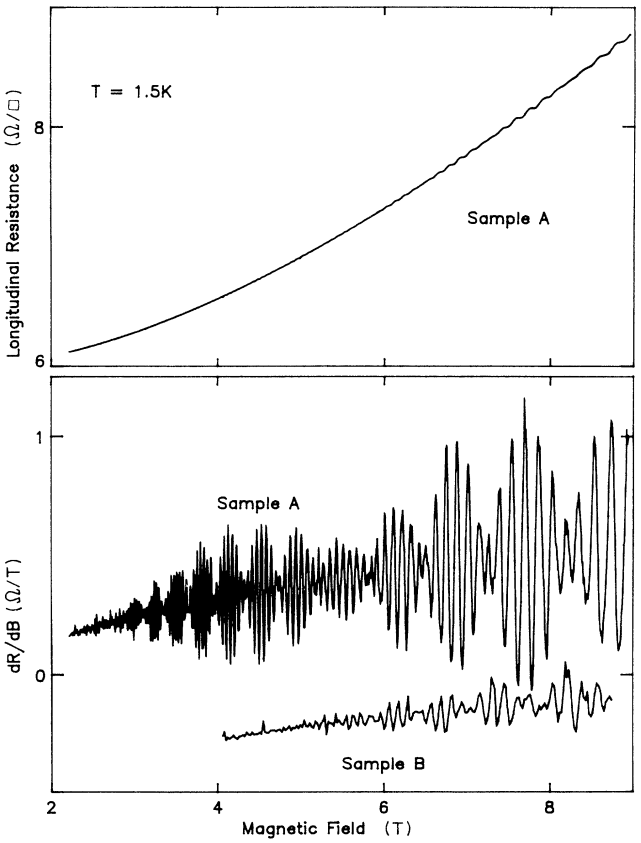

FIG. 3. Longitudinal magnetoresistance at 1.5 K and the first derivative displaying Shubnikov–de Haas oscillations for sample A. Also shown are the Shubnikov–de Haas oscillations for sample B.

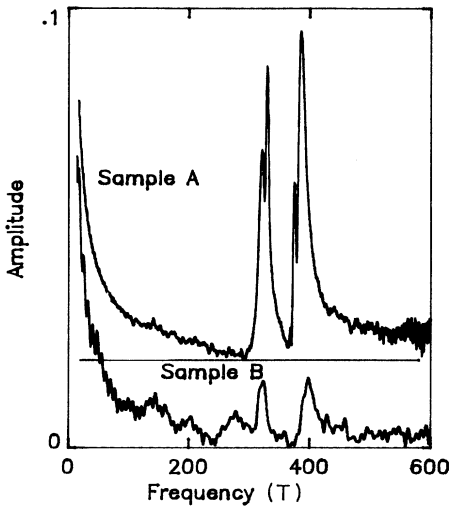

FIG. 4. Fourier transform of the first derivative of the Shubnikov–de Haas oscillations shown in Fig. 3.

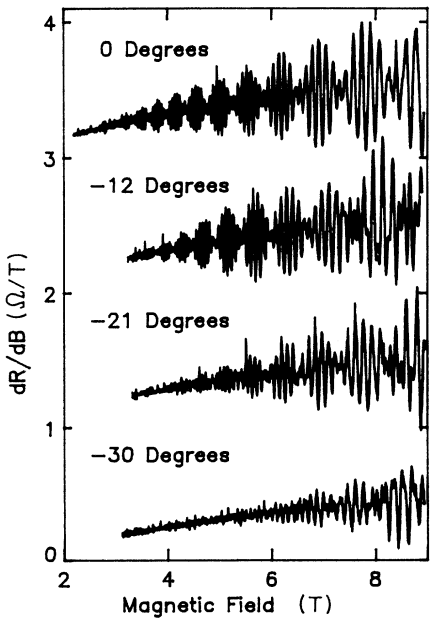

FIG. 5. Shubnikov–de Haas oscillations as a function of the orientation of the applied magnetic field with respect to the surface normal which is (001). The field is rotated toward the (110) direction.

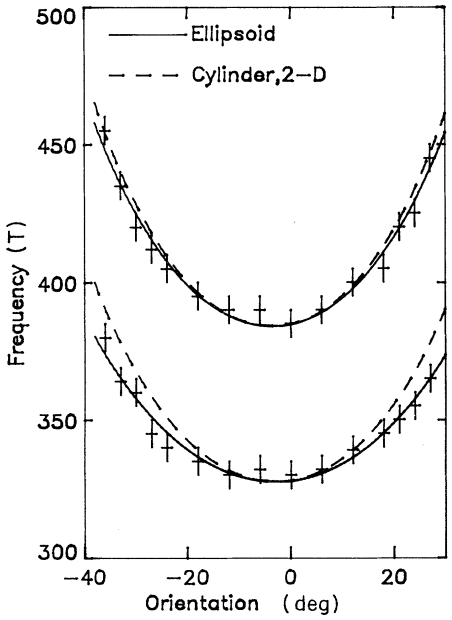

FIG. 6. Angular dependence of the two dominant Shubnikov–de Haas frequencies. The solid curve shows the fit to ellipsoids of revolution while the dashed lines show the behavior predicted by two-dimensional confinement or a cylindrical cross section.

There is also a weaker and much slower variation in the amplitude with a minimum around 5 T that does not appear in the Fourier transform except as a weak structure on the low-frequency side of the two peaks. We have no explanation for this long-period beat.

The angular dependence of the SdH oscillations are shown in Fig. 5. The position of the strong peaks that appear in the Fourier transform are plotted versus angle in Fig. 6. The strong angular variation displayed suggests an ellipsoidal or cylindrical piece of Fermi surface, but we will show later that the dependence is best described by quantum confinement.

IV. DISCUSSION

A. Hall mobility

In an earlier publication[11] we fitted the magnetoresistance at low temperatures to a simple model consisting of an isotropic electron and hole system with different densities and mobilities. The fit returned comparable electron and hole densities with mobilities less than <1000 cm^{-2}/V sec. Here we choose to test the band structure proposed by Hasegawa and Yanase[16] and assume that we have an isotropic hole Fermi surface centered at Γ with hole density $n_h = n$ and mobility μ_h, and three equivalent ellipsoidal electron Fermi surfaces at X with electron density $n_e = \frac{1}{3}n$ and anisotropic electron mobilities $\mu_{e,1}$ and

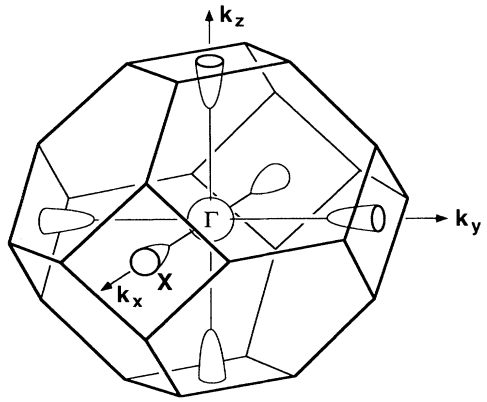

FIG. 7. Brillouin zone and the hole and electron Fermi surfaces that are used to model the magnetotransport data.

$\mu_{e,2}$, which characterize the electron mobility along and perpendicular to the axis of the ellipsoid of revolution (see Fig. 7).

The conductivity tensor is given by

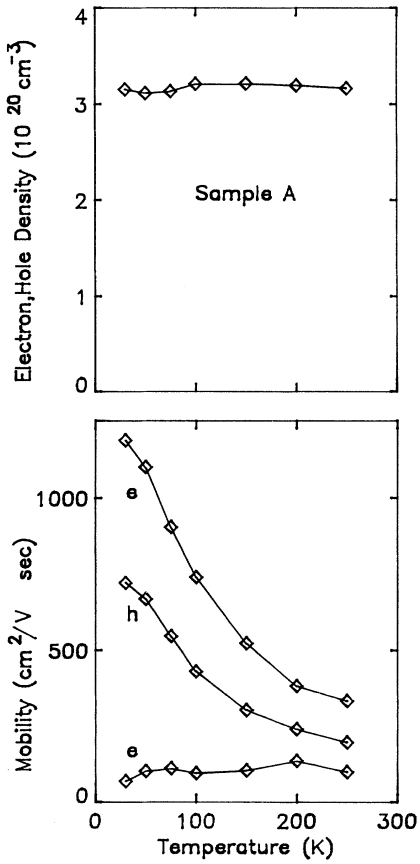

FIG. 8. Electron or hole density and mobilities extracted from the magnetoresistance data of Fig. 1 (sample A).

$$\sigma_{xx}=\frac{ne\mu_h}{1+(\mu_h B)^2}+\frac{1}{3}\frac{ne\mu_{e,2}}{1+\mu_{e,1}\mu_{e,2}B^2}+\frac{1}{3}\frac{ne\mu_{e,1}}{1+\mu_{e,1}\mu_{e,2}B^2}+\frac{1}{3}\frac{ne\mu_{e,1}}{1+(\mu_{e,1}B)^2},$$

$$\sigma_{xy}=\frac{ne\mu_h(\mu_h B)}{1+(\mu_h B)^2}+\frac{2}{3}\frac{ne\mu_{e,2}(\mu_{e,1}B)}{1+\mu_{e,1}\mu_{e,2}B^2}+\frac{1}{3}\frac{ne\mu_{e,1}(\mu_{e,1}B)}{1+(\mu_{e,1}B)^2}, \quad (1)$$

$$\sigma_{yy}=\sigma_{xx}.$$

e and B are the electron charge and magnetic field, respectively.

Magnetoresistance measurements in the Hall geometry determine the two components of the resistivity tensor, ρ_{xy} and ρ_{xx}, but they are related to σ_{xy} and σ_{xx} by

$$\rho_{xx}=\frac{\sigma_{yy}}{\sigma_{xx}\sigma_{yy}+\sigma_{xy}^2},$$

$$\rho_{xy}=\frac{-\sigma_{xy}}{\sigma_{xx}\sigma_{yy}+\sigma_{xy}^2}. \quad (2)$$

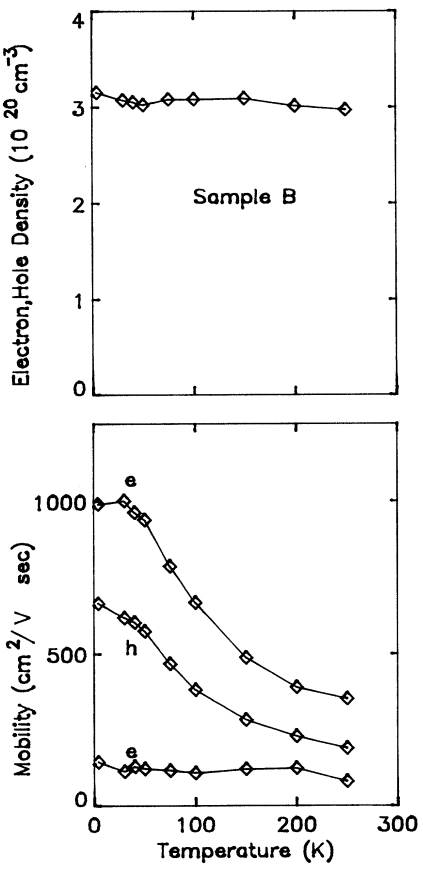

FIG. 9. Electron or hole density and mobilities extracted from the magnetoresistance data of Fig. 1 (sample B).

A satisfactory least-squares fit to the data is obtained by adjusting n, μ_h, $\mu_{e,1}$, and $\mu_{e,2}$ and displayed in Figs. 1 and 2.

Figures 8 and 9 show the temperature dependence of the hole and electron densities and mobilities for the samples A and B. Although the magnetoresistance data are relatively featureless (it basically contains a resistance, a Hall resistance, and the magnetic-field dependence of both), the parameters that are returned by the fit appear quite reasonable. The fact that the fit density in both samples is relatively temperature independent, in the face of the strong temperature dependence of the Hall resistance, establishes confidence in the parametrization.

B. Shubnikov–de Haas oscillations

Tipping the magnetic field away from the [001] direction toward the [110] might be expected to indicate the shape of the Fermi surface but this is not the case for these 20-nm-thick samples. Figure 6 shows the angular variation of the *apparent* extremal cross section represented by the two frequencies in Fig. 4 for sample A. A fit of the angular dependence to a three-dimensional model based on an ellipsoid of revolution gives the following cross sections and ratios of major to minor axes for sample A:

frequency 330±5 T, eccentricity 2.25 ,

frequency 385±5 T, eccentricity 3.80 .

This would lead one to believe that the surface in question is the electron surface that emerges from the band-structure theory of Hasegawa and Yanase[16] and is located at the X points. But we also show in Fig. 6 the result assuming a cylindrical Fermi surface. There is little to distinguish between a cylinder and an ellipsoid of revolution in the range of angles over which the SdH oscillations are observed.

A critical issue is the angular range over which the SdH oscillations can be seen. The amplitude of the SdH oscillations should rapidly diminish as the magnetic field is rotated away from the surface normal due to the collisions of the orbiting electrons with the surfaces of the thin epitaxial film. Assuming a circular orbit, the classical trajectory in real space is related to the trajectory in **k** space by

$$r=\frac{\hbar}{eB}k_F, \quad (3)$$

where r is the real-space radius and k_F is the extremal Fermi wave vector. The condition that the electron orbit fit inside the epilayer is given by

$$B>2\frac{\hbar k_F}{et}\sin\theta, \quad (4)$$

where t is the thickness of the film.

This result is not very demanding, for it assumes that the orbit will just fit into the epitaxial film. There are, of course, many similar orbits that are not centered on the film which will collide with the boundaries of the film. As a result, this inequality sets a lower bound at which

there is a vanishingly small number of electrons that do not collide with the surface. This criterion is shown in Fig. 10.

Also shown in Fig. 10 is the apparent magnetic field below which the oscillations disappear in the experimental data. There is a glaring discrepancy between the observation of the oscillations and the prediction that the three-dimensional orbit will collide with the surface. We are forced to accept the fact that the electron moves in a size-quantized orbit, constrained to move in the plane of the epitaxial layer. The angular dependence reflects the fact that only the normal component of the magnetic field controls the period of the SdH oscillations and the oscillatory transport in Figs. 3 and 5 are *quasi-two-dimensional.* This behavior has recently also been documented in work by Song *et al.*,[18] where they observe quantum-confined SdH oscillations for relatively thick (~ 100 nm) layers of gray tin.

There are many electronic subbands occupied in the 20-nm-thick film. In Fig. 11 we show the dispersion of the energy for the electronic subbands derived from the electron pocket directed along the surface normal. We have assumed that the light mass in the plane of the layer is $m^*/m_0=0.17$ and the heavy mass normal to the surface is $m^*/m_0=1$. The smallest energy splitting, between the ground state and first excited state, is of the order of 1 meV. Provided that the component of the tipped magnetic field in the plane of the film, which mixes various electric subbands, is sufficiently small, the electron states will remain quasi-two-dimensional and the angular dependence of the Shubnikov–de Haas oscillations will simply be given by the projection of the magnetic field on the surface normal. At this time we have no quantitative description of the quasi-two-dimensional quantum transport in tipped magnetic fields and must be satisfied with these heuristic arguments. Nonetheless, the observation of the oscillations at magnetic fields substantially above the critical field for three-dimensional motion constrains us to work with quantum-confined models.

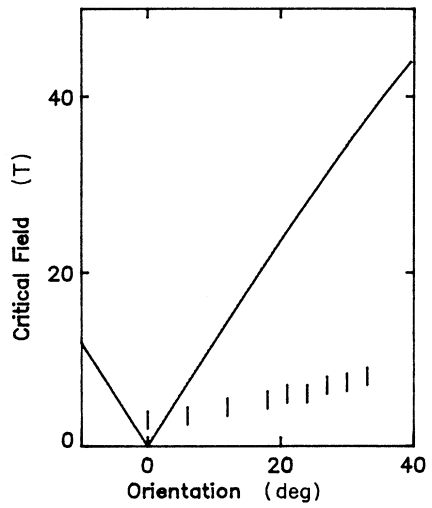

FIG. 10. Critical field required to just fit an orbit inside the epitaxial film at a tip angle θ. Experimental points are the smallest magnetic field at which Shubnikov–de Haas oscillations are seen (see Fig. 5.)

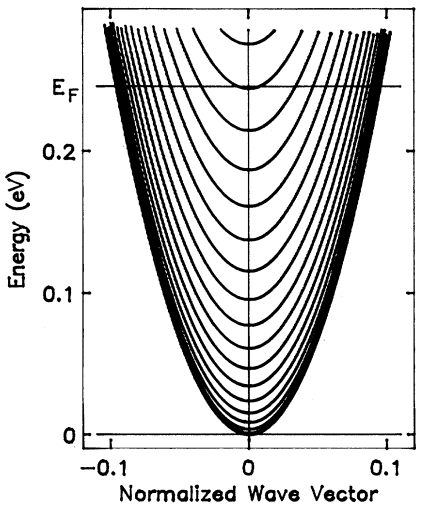

FIG. 11. Energy vs the normalized wave vector, $ka/2\pi$, for the electric subbands in a 20-nm-thick film.

By fitting the amplitude of the Shubnikov–de Haas oscillations as a function of temperature and magnetic field we can extract a measure of the effective mass and scattering rate. To do this, we model the amplitude using a modification of Ando's[19] theory for two-dimensional Shubnikov–de Haas oscillations.

Since the oscillatory component of the conductivity is small compared with the background, we assume a constant relaxation time and use the result that does not include the self-consistent aspects of the calculation. Under these assumptions the contribution to the conductivity from a single electronic subband is

$$\sigma_{xx}=\frac{N_{s,n}e^2\tau}{m_1}\frac{1}{1+(\omega_c\tau)^2}\times\left[1+2\frac{2\pi^2k_BT}{\hbar\omega_c}\operatorname{csch}\left[\frac{2\pi^2k_BT}{\hbar\omega_c}\right]\times\cos\left[\frac{2\pi\mu_n}{\hbar\omega_c}\right]\exp\left[-\frac{\pi}{\omega_c\tau}\right]\right]. \quad (5)$$

Here $N_{s,n}$ is the two-dimensional subband density for the nth subband and

$$\mu_n=\mu-n^2\frac{\hbar^2}{2m_0}\frac{\pi^2}{t^2}=\mu-n^2\hbar\omega_0\,, \quad (6)$$

where μ is the Fermi energy, t is the film thickness, and m_0 is the electron mass along the growth direction. $\hbar\omega_c$ is the cyclotron energy given by $\hbar eB/m_1$ and m_1 is the

in-plane mass.

For convenience, we assume in the following that the conductivity is dominated by a single set of electronic subbands corresponding to one set of carriers in the semimetallic film. To find the conductivity we simply sum over all the occupied electronic subbands.

If we approximate the summation by an integral, $\sum_n \rightarrow \int dn$, we find for the conductivity

$$\sigma_{xx} \approx N_v t \frac{e^2\tau}{m_1}\frac{1}{1+(\omega_c\tau)^2} + N_s \frac{e^2\tau}{m_1}\frac{1}{1+(\omega_c\tau)^2}\left[\frac{\hbar\omega_c}{2\hbar\omega_0}\right]^{1/2}\frac{2\pi^2 k_B T}{\hbar\omega_c}\operatorname{csch}\left[\frac{2\pi^2 k_B T}{\hbar\omega_c}\right]\cos\left[\frac{2\pi\mu}{\hbar\omega_c}-\frac{\pi}{4}\right]\exp\left[-\frac{\pi}{\omega_c^{\tau}}\right] . \quad (7)$$

Equation (7) has the functional form for the three-dimensional Shubnikov–de Haas oscillations arising from an extremal section of the Fermi surface.

The data displayed in Fig. 3 are the first derivative of the transverse resistivity which is dominated by the rapidly varying part of Eq. (7). Since $\rho_{xy} \ll \rho_{xx}$, $(1/\rho)\partial\rho/\partial B = -(1/\sigma)\partial\sigma/\partial B$ and we recover the following expression for the first derivative of the Shubnikov–de Haas oscillations:

$$\frac{1}{\rho}\frac{d\rho}{dB} \approx \frac{1}{B}\frac{N_s}{N_v t}\frac{2\pi\mu}{\hbar\omega_c}\left[\frac{\hbar\omega_c}{2\hbar\omega_0}\right]^{1/2}\frac{2\pi^2 k_B T}{\hbar\omega_c} \times \operatorname{csch}\left[\frac{2\pi^2 k_B T}{\hbar\omega_c}\right]\cos\left[\frac{2\pi\mu}{\hbar\omega_c}-\frac{3\pi}{4}\right] \times \exp\left[-\frac{\pi}{\omega_c\tau}\right] , \quad (8)$$

where N_v is the volume density of carriers.

We have fitted the temperature and field dependence of the oscillations with Eq. (8) allowing the scale, the mass m_1, and the scattering time τ to vary. We pick the magnetic-field positions at which to fit the amplitude to be between the nodes of the strong beat pattern. We simply ignore the slow beat pattern and the least-squares-fit averages of this slow amplitude variation.

The fit returns

$$m_1 = 0.17 m_e$$

and

$$\tau = 1.62 \times 10^{-13} \text{ s} .$$

The latter corresponds to a mobility of 1700 $\text{cm}^2/\text{V sec}$ which is comparable to the low-temperature mobility extracted from the magnetotransport.

The extracted τ is sensitive to the magnetic-field dependence of the prefactor in Eq. (8). In particular if we take the simple two-dimensional form, the prefactor changes by $B^{1/2}$ and the fit returns the same mass but a different scattering time which corresponds to a mobility of 1400 $\text{cm}^2/\text{V sec}$.

In Fig. 12 we plot the fit amplitude versus the experimental amplitude for data for magnetic fields from 2 to 9 T and temperatures from 1.5 to 20 K. The apparent scatter and failure to fall along the straight line in the figure is primarily due to the slow beat which is not modeled and completely ignored in the fit.

In Figs. 13–16 we show the experimental data and the fit. If we ignore for the moment the fast and slow beat, the overall temperature and magnetic-field dependence are well described by the mass and scattering time extracted from the fit.

Since we have already pointed out the fallacy of using the angular dependence to determine the shape of this piece of Fermi surface, we must rely on the inferred mobility and mass to assign it to the electron pocket directed towards X, [001]. The mobility is in rough agreement with the light-mass direction derived from the magnetotransport. It is probably the smallest Fermi-surface cross section and would be expected to be the most easily observed especially since it also appears to have the highest mobility in the magnetotransport. The mass of $0.17 m_0$ is close to the mass calculated by Hasegawa and Yanase, $0.1 m_0$. As a result we assign this oscillation to the pocket of electrons directed towards X.

We return for a moment to the quasi-two-dimensional character of the Shubnikov–de Haas oscillations. The reader should be struck by the fact that the fit we have made to the quantum oscillations is essentially three-dimensional despite the fact that the angular dependence demands that we think of quantum confined orbits in the magnetic field. Ideally we would expect the two-dimensional character also to manifest itself as a series of different Shubnikov–de Haas periods, one for each of the

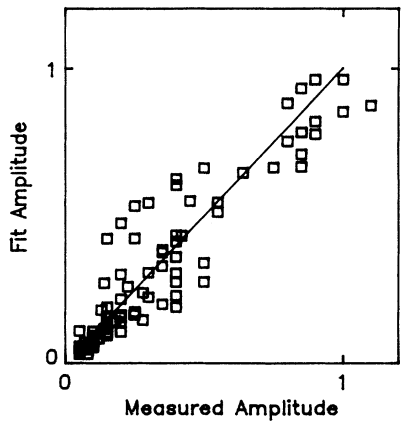

FIG. 12. Fit amplitude vs measured amplitude obtained by fitting the magnetic-field dependence and temperature dependence of the Shubnikov–de Haas oscillations to Eq. (8).

occupied electric subbands. In Eq. (8) we have approximated the sum by an integral and have tacitly assumed that the individual contributions to the quantum oscillations are sufficiently broad that they overlap. Indeed, the Fourier transform reveals no fine structure with the exception of a small feature on the low-frequency side. This is acceptable. What is difficult to reconcile is the fact that while the quantum confinement cannot be resolved in the SdH it is strong enough to enforce the quantum-confined angular dependence displayed in Figs. 6 and 10. We cannot resolve this apparent contradiction at this time.

Exchange splitting. We interpret the strong beat between the quantum oscillations as a splitting of the conduction band caused by the exchange interaction of the nearly fully polarized $4f$ spin on the Er^{3+} with the conduction electrons. The splitting is given by $(\mu_\uparrow - \mu_\downarrow) = \Delta B \hbar e / m_1$, where $\mu_\uparrow$ and $\mu_\downarrow$ are the Fermi levels measured from the spin-up and spin-down conduction-band bottoms, respectively.

We find the following for the two samples investigated. For sample A,

$$(\mu_\uparrow - \mu_\downarrow) = 38 \pm 7 \text{ meV}$$

and for sample B,

$$(\mu_\uparrow - \mu_\downarrow) = 55 \pm 7 \text{ meV} .$$

If we normalize these results by the Er concentration in each sample we obtain a splitting of 67 ± 12 meV and 81 ± 10 for samples A and B, respectively, scaled to 100%. The splittings appear to scale, within experimental error, with the Er concentration which is consistent with the hypothesis that the splitting arises from the interaction of the conduction electrons with the Er $4f$ spins.

Upon closer examination of the beating in the experimental data, it becomes apparent that the nodes of the beat pattern are not perfectly periodic in $1/B$. Furthermore, as the temperature is raised, the phase of the beat pattern shifts and the period is extended as can be seen in Figs. 13–16. The vertical lines that are drawn in these figures are keyed to the model calculation that assumes a constant exchange splitting. With these as a guide the lack of periodicity in $1/B$ and the shift with temperature are readily apparent. This effect is rendered in a quantitative manner in Fig. 17 where the nodes are indexed and plotted versus $1/B$. The data fail to fall on a straight line and the apparent periodicity changes as the sample is warmed.

A reasonable explanation for this behavior is the fact

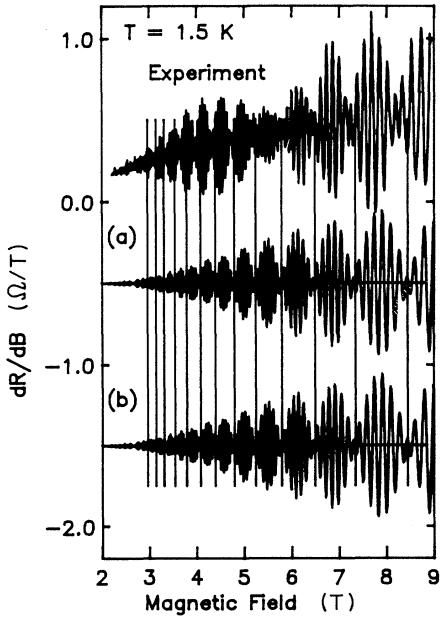

FIG. 13. dR/dB vs the magnetic field at 1.5 K. The top curve is the experimental data. The middle curve is the fit with a constant splitting. The bottom curve is a fit with a splitting proportional to the magnetization of the Er $4f$ spin. The vertical lines are fixed at the nodes of the fit with constant splitting, the middle curve (a), and serve to guide the eye as the beat pattern in the experimental data and the model splitting proportional to the Er magnetization (b) change at low field and high temperature.

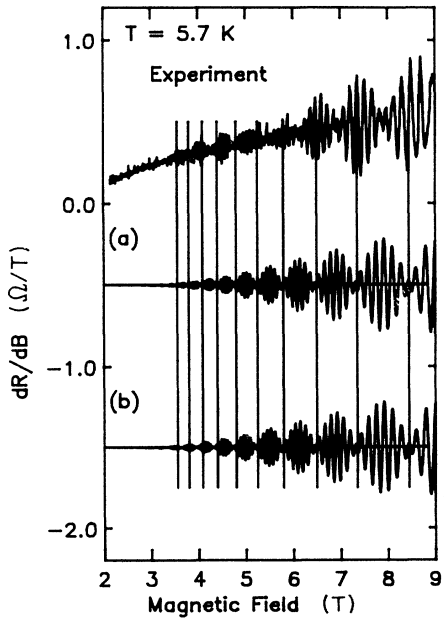

FIG. 14. dR/dB vs the magnetic field at 5.7 K. The top curve is the experimental data. The middle curve is the fit with a constant splitting. The bottom curve is a fit with a splitting proportional to the magnetization of the Er $4f$ spin. The vertical lines are fixed at the nodes of the fit with constant splitting, the middle curve (a), and serve to guide the eye as the beat pattern in the experimental data and the model splitting proportional to the Er magnetization (b) change at low field and high temperature.

that the polarization of the Er spin which causes the exchange splitting of the conduction band depends on temperature and magnetic field. In the following we explore the consequences of this by examining the periodic part of Eq. (8). We assume that it can be represented by the sum of two oscillatory functions representing the spin-up and spin-down electrons at the Fermi surface,

$$\cos\left[\frac{2\pi\mu_\uparrow}{\hbar\omega_c}+\phi\right]+\cos\left[\frac{2\pi\mu_\downarrow}{\hbar\omega_c}+\phi\right] .$$

The relative Fermi energies $\mu_\uparrow$ and $\mu_\downarrow$ are given by

$$\mu_{\uparrow\downarrow}=\mu\pm\tfrac{1}{2}g^0\mu_B H_{\rm int}\pm\tfrac{1}{2}\lambda\langle S\rangle . \tag{9}$$

Here μ is the Fermi energy ignoring the spin splitting, the second term is the spin splitting in the internal magnetic field (the applied field reduced by demagnetizing the field caused by the polarization of the Er spins), and the last term is the exchange splitting of the conduction band caused by the interaction of the conduction electrons with the thermal average Er $4f$ spin, $\langle S\rangle$. g^0 is the bare-conduction-electron g factor and μ_B is the Bohr magneton. The exchange-induced splitting completely dominates the spin splitting and in the following we ig-

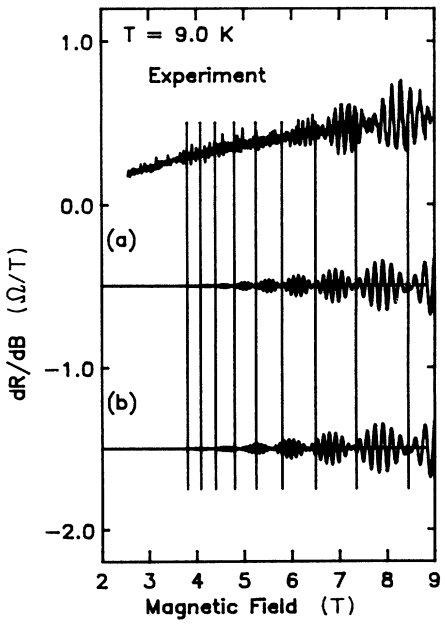

FIG. 15. dR/dB vs the magnetic field at 9.0 K. The top curve is the experimental data. The middle curve is the fit with a constant splitting. The bottom curve is a fit with a splitting proportional to the magnetization of the Er $4f$ spin. The vertical lines are fixed at the nodes of the fit with constant splitting, the middle curve (a), and serve to guide the eye as the beat pattern in the experimental data and the model splitting proportional to the Er magnetization (b) change at low field and high temperature.

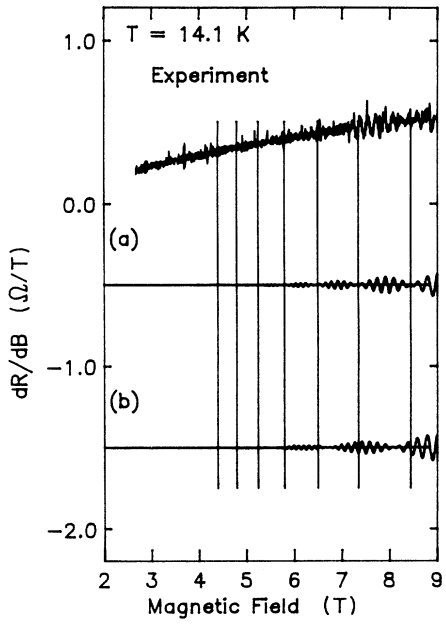

FIG. 16. dR/dB vs the magnetic field at 14.1 K. The top curve is the experimental data. The middle curve is the fit with a constant splitting. The bottom curve is a fit with a splitting proportional to the magnetization of the Er $4f$ spin. The vertical lines are fixed at the nodes of the fit with constant splitting, the middle curve (a), and serve to guide the eye as the beat pattern in the experimental data and the model splitting proportional to the Er magnetization (b) change at low field and high temperature.

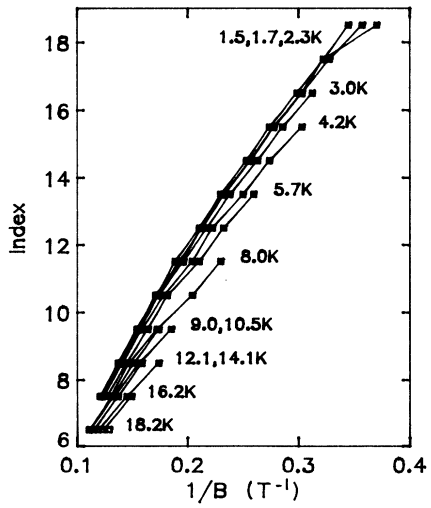

FIG. 17. Nodes of the beat pattern in the Shubnikov–de Haas oscillations vs $1/B$ with temperature as a parameter.

nore the conduction-band spin splitting caused by the internal magnetic field.

The beat pattern can then be simply modeled as follows:

$$\cos\left[\frac{2\pi\mu}{\hbar\omega_c}+\phi\right]\cos\left[\frac{2\pi\Delta\mu}{\hbar\omega_c}\right],$$

where $\Delta\mu=\frac{1}{2}\lambda\langle S\rangle$. The zeros of the beat pattern can then be indexed by

$$2\Delta\mu/\hbar\omega_c=l+\tfrac{1}{2} \tag{10}$$

or

$$\lambda\langle S\rangle/\hbar\omega_c=l+\tfrac{1}{2}\,, \tag{11}$$

where l is an integer and $\omega_c=eB_l/m_1$.

If we assume that the Er spin is fully polarized at high fields and low temperatures, the slope of the line shown in Fig. 17 determines the fully polarized exchange splitting of the conduction band for sample A. It is the same parameter extracted from the splitting revealed in the Fourier transform in Fig. 4 and ~38 meV. The collapse of the fan diagram in Fig. 17 is ascribed to the reduction in $4f$ spin polarization as the sample is heated or the field is reduced.

We can extract the temperature and field dependence of the exchange splitting by using Eq. (11). In particular, we note that the exchange splitting at temperature T at a given zero or node of the beat pattern $B_l(T)$ is given by

$$\lambda\langle S(B,T)\rangle=(l+\tfrac{1}{2})(\hbar e/m_1)B_l(T)\,. \tag{12}$$

In Fig. 18 we display the exchange splitting as a function of magnetic field and temperature, derived from this inversion of the data. Although the splitting can be extracted only over a limited range of magnetic fields and

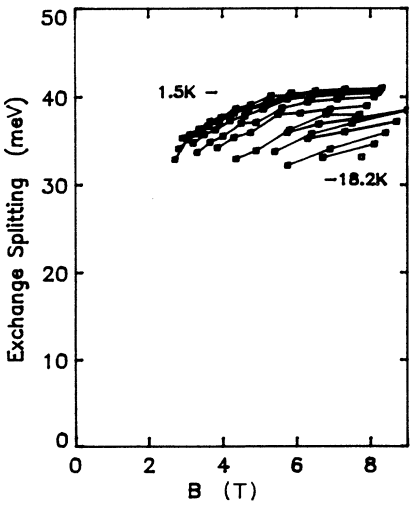

FIG. 18. Exchange splitting vs the magnetic field with temperature as a parameter deduced from Fig. 17.

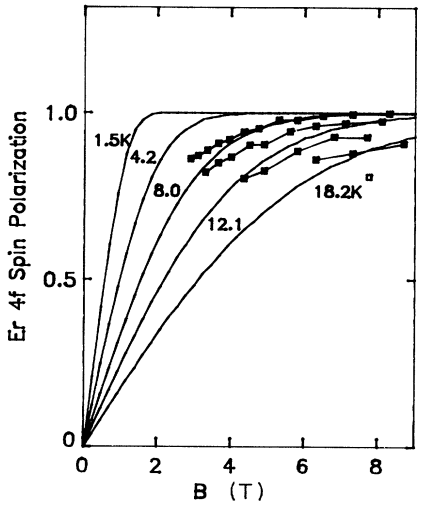

FIG. 19. Magnetization of the Er $4f$ spin vs the magnetic field normal to the film. We assume a magnetic moment of $5.3\mu_B$ and correct the internal field for demagnetization but have not included exchange interaction between the $4f$ spins. The experimental data are selected from Fig. 18 for comparison.

temperature it has the qualitative appearance of the magnetization curves for an isolated spin in an applied field with temperature as a parameter modeled and displayed in Fig. 19.

The behavior predicted in Fig. 19 does not agree in detail with that shown in Fig. 18. (We also compare with experiment directly, in Figs. 13–16 by showing the predicted beat pattern that emerges from this model of the temperatures- and magnetic-field-dependent exchange splitting.) The experimental data shown in Fig. 19, selected to contrast with this simple model, while showing the correct qualitative features, fall too rapidly as the temperature is raised or as the field is reduced. This may reflect the fact that the Er magnetization does not fit a simple Brillouin function. Indeed, such a model is expected to be an oversimplification and does not even include the exchange interaction between the Er spins (see Chroboczek *et al.*[20]). We make no attempt here to use or develop more sophisticated models of the Er magnetization as a function of temperature and magnetic field.

We can compare the magnitude of the exchange splitting deduced from the SdH oscillations with that determined from the spin-disorder-scattering contribution to the resistivity.[11] For the latter we have

$$\Delta\rho_s=2\pi^2(k_f/ne^2)(m^2\Gamma^2/h^3)n_s(\tfrac{1}{4})\,, \tag{13}$$

where Γ is the exchange parameter in the Hamiltonian $\Gamma S_i\cdot s$. In the previous estimate for Γ we had assumed $m=m_e$ and a k_F given by the total electron or hole density of 3×10^{20} cm^{-3}. Here we recompute Γ using a mass of $0.17m_e$ and an electron density appropriate to a single electron pocket, $n=10^{20}$ cm^{-3}. k_F is 1.09×10^9 m^{-1}. With these parameters Γ is found to be substantially larger than the previous estimate and approximately

equal to 7.3 eV Å^3. However, λ is related to Γ by $\lambda = n_s \Gamma$, where n_s is the density of Er spins. Using the above value for Γ, 7.3 eV Å^3, the predicted splitting of the conduction band, for fully polarized Er spins, is $\sim$42 meV, for sample A, $Sc_{0.43}Er_{0.57}$. This is reasonably close to the saturated exchange splitting shown in Fig. 18.

V. CONCLUSIONS

Magnetotransport measurements are consistent with the band-structure model of Hasegawa and Yanase[16] which predicts semimetallic transport on a Fermi surface consisting of electron pockets at X and holes at Γ. The lattice-matched $Sc_{1-x}Er_xAs$ alloy reveals Shubnikov–de Haas oscillations that most likely arise from the electron pocket at X directed along the surface normal. Remarkably the oscillations persist when the magnetic field is tipped away from the surface normal to the point that three-dimensional cyclotron orbits must collide with the surface of the film. This compels us to conclude that the Shubnikov–de Haas oscillations arise from orbits that are quantum confined by the finite thickness of the epitaxial film. The temperature and magnetic-field dependence of the oscillations allow us to determine a mass of $0.17m_e$ and a scattering rate that is consistent with the Hall mobility. The strong beating in the Shubnikov–de Haas oscillations arises from an exchange splitting of the conduction band at X caused by interactions with the Er $4f$ spins. The exchange interaction deduced from the Shubnikov–de Haas oscillations agrees with that determined from spin-disorder scattering.

An important issue that remains and can be addressed by buried semimetal layers such as $Sc_{1-x}Er_xAs$ is the effect of quantum confinement on the electronic properties of semimetals. Earlier, we reported preliminary results[12] on the resistance of ultrathin films and noted the apparent absence of a semimetal-to-semiconductor transition as the electron and hole states are driven apart. This behavior is not expected on the basis of simple confinement effects[21] and needs to be explored with very large magnetic fields. Surface scattering suppresses the mobility in thin films and only magnetotransport in the highest magnetic fields will give any information on the relative contribution to the transport from the electrons and holes. Another issue that is of great technological importance is vertical transport through thin semimetal films which would address their potential as metal-base transistors.

*Present address: Walter Schottky Institute, Technische Universität München, Garching, West Germany.

[1]T. Sands, J. P. Harbison, W. K. Chan, S. A. Schwarz, C. C. Chang, C. J. Palmstrøm, and V. G. Keramidas, Appl. Phys. Lett. **52**, 1216 (1988).

[2]C. J. Palmstrøm, C. C. Chang, A. Yu, G. J. Galvin, and J. W. Mayer, J. Appl. Phys. **62**, 3755 (1987).

[3]A. M. Wowchak, J. N. Kuznia, and P. I. Cohen, J. Vac. Sci. Technol. B **7**, 733 (1989).

[4]S. A. Chambers, J. Vac. Sci. Technol. B **7**, 737 (1989).

[5]C. J. Palmstrøm, B.-O. Fimland, T. Sands, K. C. Garrison, and R. A. Bartynski, J. Appl. Phys. **65**, 4753 (1989).

[6]A. Guivarc'h, R. Guérin, and M. Secoué, Electron. Lett. **23**, 1004 (1987).

[7]C. J. Palmstrøm, N. Tabatabaie, and S. J. Allen, Jr., Appl. Phys. Lett. **53**, 2608 (1988).

[8]C. J. Palmstrøm, K. C. Garrison, S. Mounier, T. Sands, C. L. Schwartz, N. Tabatabaie, S. J. Allen, Jr., H. L. Gilchrist, and P. F. Miceli, J. Vac. Sci. Technol. B **7**, 747 (1989).

[9]H. J. Richter, R. S. Smith, N. Herres, N. Seelmann-Eggebert, and Wenekers, Appl. Phys. Lett. **53**, 99 (1988).

[10]J. D. Ralston, H. Ennen, P. Wennekers, P. Hiesinger, N. Herres, J. Schneider, H. D. Müller, W. Rothemund, F. Fuchs, J. Schmälzlin, and K. Thonke, J. Electron. Mater. **19**, 555 (1990).

[11]S. J. Allen, Jr., N. Tabatabaie, C. J. Palmstrøm, G. W. Hull, T. Sands, F. DeRosa, H. L. Gilchrist, and K. C. Garrison, Phys. Rev. Lett. **62**, 2309 (1989).

[12]S. J. Allen, Jr., N. Tabatabaie, C. J. Palmstrøm, G. W. Hull, T. Sands, F. DeRosa, H. L. Gilchrist, and K. C. Garrison, Surf. Sci. **228**, 13 (1990).

[13]A. Guivarc'h, J. Caulet, and A. Le Corre, Electron. Lett. **25**, 1050 (1989).

[14]A. Le Corre, J. Caulet, and A. Guivarc'h, Appl. Phys. Lett. **55**, 2298 (1989).

[15]A. Guivarc'h, A. Le Corre, J. Caulet, B. Guenais, M. Minier, G. Ropars, P. A. Badoz, and J. Y. Duboz, Mater. Res. Soc. Symp. Proc. **160**, 331 (1990).

[16]A. Hasegawa and A. Yanase, J. Phys. Soc. Jpn. **42**, 492 (1977).

[17]C. J. Palmstrøm, S. Mounier, T. G. Finstad, and P. F. Miceli, Appl. Phys. Lett. **56**, 382 (1990).

[18]S. N. Song, X. J. Yi, J. Q. Zheng, Z. Zhao, L. W. Tu, G. K. Wong, and J. B. Ketterson, Phys. Rev. Lett. **65**, 227 (1990).

[19]T. Ando, J. Phys. Soc. Jpn. **37A**, 1233 (1974).

[20]J. A. Chroboczek, P. A. Badoz, F. Arnaudd'Avitaya, A. Guivarc'h, A. Corre, W. Joss, A. Briggs, S. Auffret, and J. Pierre, Proceedings of the 20th International Conference of the Physics of Semiconductors, Thessaloniki, 1990 (World Scientific, Singapore, 1990), pp. 2291.

[21]J. B. Xia, S. F. Ren, and Y. C. Chang, Phys. Rev. B **43**, 1692 (1991).